ORIGINAL PAPER

Biobased Immiscible Polylactic Acid (PLA): Poly(3-hydroxybutyrate-co-3-hydroxyvalerate) (PHBV) Blends: Impact of Rheological and Non-isothermal Crystallization on the Bead Foaming Behavior

Christian Brütting[1] · Julia Dreier[2] · Christian Bonten[1] · Holger Ruckdäschel[1,3]

Abstract

Nowadays, bead foams are of great interest due to their high lightweight potential. The processing of such foams strongly depends on the crystallization and rheological behavior of the polymers used. By blending polymers, these properties can be tailored to obtain beaded foams with low density, small cell size and high cell density. As a bio-based polymer, PLA is of great interest due to its renewable carbon source. PLA suffers from its low thermal and rheological properties, which can be compensated by using blends. The correlation between the PLA/PHBV ratio and the rheological as well as the crystallization behavior was investigated. The use of PHBV as a minor phase significantly changes the rheological properties and increases the crystallization behavior of PLA. These findings were applied to the foam extrusion process to obtain low density bead foams. Bead foams with densities below 100 kg/m^3, mean cell sizes below 50 μm and cell densities of 1×10^7 cells/cm^3 were obtained.

Keywords Biopolymer blend · Biofoam · PLA · PHBV · Bead foam extrusion · Biopolymer

Introduction

Polymer foams, especially bead foams such as expandable polystyrene (EPS) or expanded polypropylene (EPP) are a widely applied in sports as well as in the packaging industry. Use in such applications depends largely on the mechanical behavior and density of the polymer foams. While many types of bead foams have been developed, only a few are commercially available, but research in this field is increasing tremendously [1]. In general bead foams show high potential because they usually obtain low densities such as foam extruded foams and can be processed to complex geometries such as injection molding parts [2]. However up to now mainly EPS and EPP are used in industry. Due to restrictions and the low CO_2 footprint of PLA [3] it can be a promising alternative to EPS and EPP. There is limited work in the field of biobased bead foams [4–9] For example, Nofar et al. focused on a stirred autoclave method to produce expanded PLA [4, 8–10]. Another method to produce bead foams is an extrusion process [11, 12]. Although the bead foam extrusion is advantageous to other processes such as autoclave processes, no study on the bead foaming behavior of PLA or PLA-based blends in an extrusion process is available in literature.

It is well known, that the rheological properties affect the foaming behavior of polymers. The impact on rheological properties on foaming behavior has been shown for polylactic acid (PLA).[13] Here, a chain extender (an

✉ Holger Ruckdäschel
ruckdaeschel@uni-bayreuth.de

Christian Brütting
christian.bruetting@uni-bayreuth.de

Julia Dreier
julia.dreier@ikt.uni-stuttgart.de

Christian Bonten
christian.bonten@ikt.uni-stuttgart.de

1   Department of Polymer Engineering, University Bayreuth, Universitätsstraße 30, 95447 Bayreuth, Germany

2   Institut Für Kunststofftechnik, University of Stuttgart, Pfaffenwaldring 32, 70569 Stuttgart, Germany

3   Bavarian Polymer Institute and Bayreuth Institute of Macromolecular Research, University of Bayreuth, Universitätsstraße 30, 95447 Bayreuth, Germany

epoxy styrene acrylate) was used to increase the melt viscosity and induce strain hardening, which resulted in a decrease in foam density for semi-crystalline PLA. In other works, PLA was modified with epoxy-based chain extenders, which increased the melt strength, resulting in lower densities and smaller cell sizes [14–17].

In addition to rheological properties, the crystallization behavior is important for foaming [18]. Li et al. [19] investigated the foaming performance of PLA based on the non-isothermal crystallization behavior. They showed that the foaming behavior strongly depends on the foaming temperature, which determines the crystallization rate. Another work by Standau et al. [20] compared the foaming behavior of different PLA grades and showed that PLA grades with high crystallization rates can hardly be foamed. PLA foams with expansion ratios of 15–30 and average cell sizes of 80–270 μm were obtained. Moreover, the presence of CO_2 affects the thermal properties of polymers, resulting in lower glass transition temperatures, lower crystallization temperatures, and higher crystallization rates [21–27]. Methods to improve the crystallization rate include the use of chain extenders [28–30] to create branches that serve as nucleation sites, the addition of inorganic nucleating agents [31–34] or blending with other polymers [35].

In addition to the rheological properties and crystallization behavior, the processing conditions also influence the foaming behavior. However, the processing of polymer foams is influenced by the temperature, the type of blowing agent, the concentration of the blowing agent and many other parameters. Here, it is almost impossible to holistically describe all parameters and their effects on the foaming behavior. Recently, an attempt was made to use machine learning (ML) for an autoclave foaming process to model the processing behavior of different types of PLA with different properties at different process conditions. The foaming performance of unmodified PLA could be predicted based on different material properties and process parameters [36]. However, a lot of data is required for the application of machine learning, which limits its application.

As mentioned earlier, one method to overcome the drawbacks of PLA is blending with other polymers. The group of polyhydroxyalkanoates (PHA) offers an excellent opportunity to be used as blending partners for PLA. PHAs are biobased and biodegradable in all natural environments, e.g., marine, freshwater, soil, domestic and industrial composting. In addition, PHAs are resistant to hydrolysis, have good barrier properties to gases are UV resistant, and insoluble in water. The most common PHA is polyhydroxybutyrate (PHB), followed by a copolymer of PHB and polyhydroxyvalerate (PHV),

PHBV. Due to its biodegradability, PHA offers aerobic and anaerobic end-of-life pathways, but recycling (e.g. mechanical recycling) is also a potential option in terms of circular economy and life cycle assessment [37–41].

For foaming, rheological properties are an important feature. Unmodified PLA behaves viscoelastically and has low melt elasticity and low melt strength. Blending can improve the rheological properties. Some work has been done on PLA/PHA blends in the past. Pietrosanto et al. [42] were able to show that increasing the PHB content in the blending system leads to an increase in zero shear viscosity and an more pronounced shear thinning behavior, which can be associated with an increase in chain branching and molecular weight distribution [42]. Another work has shown that rheological measurements indicate an increase in the storage modulus and loss modulus of the PHBV matrix with the addition of PLA [43] but also that the thermal instability of PHB has a major impact on rheological performance [44].

The mixing of polymers also has an important influence on the crystallization behavior, as one polymer can significantly affect the crystallization of the other polymer. In the case of PLA, the crystallization kinetics depend on the composition of the blend component. PLA has a slow crystallization rate [30, 45, 46] which has led to several works addressing the improvement of these properties, e.g., by adding nucleating agents [30, 45, 47, 48]. Mixing with PHA also leads to a change in crystallization behavior [49]. Gasmi et al. showed an inhibition of PHBV crystallization by PLA [47] which leads to the fact that PHBV, in contrast, can act as a nucleating agent for PLA, thus promoting its crystallization [50, 51]. A previous study [49] about blends containing PLA and PHBV shows, how the composition is affecting the foaming behavior in a solid-state autoclave foaming process. It was worked out, how the addition of PHBV changed the crystallizing and the dynamic mechanical properties, which was correlated to the foaming behavior. It was shown, that PHBV could increase the cell and the nucleation density at similar processing conditions. Additionally it was shown, that the used blend system is immiscible [49].

In summary, the bead foam extrusion of PLA was not investigated so far. This study is focused on that field to extend the knowledge of the foaming behavior of PLA. To overcome the drawbacks of PLA, it will be blended with PHBV to tailor its properties and identify the impact on foaming behavior. Since the rheological and non-isothermal crystallization are in great importance for the foam extrusion process, these properties will be analyzed for different blend ratios.

Experimental

Materials

In this work, PLA Ingeo™ 2003D from NatureWorks Ltd. (*Minnetonka, Minnesota, USA*) was used. It is a high molecular weight ($M_w = 225$ kg/mol) extrusion grade with a D-content about 4.3% and a melting point at 150 °C [20]. As blend partner, the biopolymer PHBV ENMAT™ Thermoplastic Resin Y1000P from TianAn Biopolymer (*Ningbo City, Zhejiang Province, China*) with a melting point of 170 °C and a glass transition temperature of approx. 0 °C was chosen. The molecular weight of the selected PHBV is 300 kg/mol. This grade can be used in various applications like injection molding, thermoforming, blown film and extrusion. In a previous study we showed the immiscibility of the PLA/PHBV Blend with AFM measurement [49]. Prior to each measurement or processing step, the samples have been drying. PLA was dried at 60 °C and PHBV at 40 °C under vacuum for 16 h.

Rheological Analysis

The rheological properties of the polymers were analyzed by a strain-controlled rotational rheometer RDA III from TA Instruments (New Castle, DE, USA) with plate–plate geometry under nitrogen atmosphere. The samples had a diameter of 25 mm and a height of 1 mm and were analyzed isothermally at 180 ℃. Oscillatory tests were performed to obtain the complex viscosity, the storage modulus, the loss modulus, and the loss factor of all materials. Prior to measuring the frequency-dependent viscoelastic behavior, the linear viscoelastic regime was determined by strain-sweep experiments. Frequency sweeps were performed with strains of 10% from 500 to 1 rad/s. To avoid degradation during the experiments, the samples have been dried prior to the measurements.

Thermal Analysis

The crystallinity as well as the crystallization behavior was evaluated using a DSC (Mettler Toledo DSC 1, Columbus, OH). Each measurement was conducted with am amount of 2–4 mg depending on the density of the foams. The heating and cooling rates were set to 10 K/min under a nitrogen atmosphere with a flushing rate of 20 mL/min. After each heating and cooling step the samples were treated isothermally for 3 min. The temperature range was set between 25 and 200 °C. The analysis was performed with the software from Mettler Toledo.

Foam Production

A tandem extrusion line from Dr. Collin GmbH (Ebersberg, Germany) is used to process the materials. The setup consists of a twin-screw extruder (L/D = 42) with screw diameters of 25 mm and a single screw extruder (L/D = 30) with a screw diameter of 45 mm. The temperature in the twin screw extruder was set to 180 °C with a screw speed of 160 rpm. The single screw extruder set to a temperature of 140 °C and a screw speed of 12 rpm. The blowing agent (CO_2) is dosed via a gas metering station (Maximator DSD500/20/SS, Maximator GmbH, Nordhausen, Germany). The materials are processed at a throughput of 8 kg/h and a CO_2 concentration of 6 wt%. An underwater granulation unit (UWG) (LPU MAP 5, Gala Kunststoff- und Kautschukmaschinen GmbH, Xanten, Germany) is attached to the extrusion unit. The gas-laden melt is transferred to the UWG, foamed and cut by a knife head. In this section of the process, there are multiple process parameters that can be varied. In this work, the water temperature was set to 45 °C and the knife speed to 2500 rpm. No water pressure was applied, and the die diameter was 2.8 mm. The die temperature was kept constant at 160 °C for all blend variations.

Foam Analysis

The density of the polymer foam was analyzed according to the Archimedes principle on a density balance by using the following equation with ρ representing the density, A the sample weight, B the buyonce and ρ_{water} the density of the water.

$$\rho = \left| \frac{A}{B} \right| * \rho_{water} \tag{1}$$

To analyze the morphological properties scanning Electron Microscopy (SEM (JSM-6510 *JEOL, Akishima, Japan*) was used. From the SEM Images, the cell size, cell size distribution was analyzed with ImageJ (v1.48, University of Wisconsin, Madison, Wisconsin, USA). The morphological properties were calculated according to the following equations [49, 52].

$$N_0 = \left(\frac{nM^2}{A} \right)^{\frac{3}{2}} \tag{2}$$

$$N_D = \left(\frac{nM^2}{A} \right)^{\frac{3}{2}} \left(\frac{1}{\rho} \right) \tag{3}$$

Here N_o represents the cell density, M the magnification, and n the number of measured cells in the measured area

A. N_D represents the nucleation density and ρ the density of the foam.

Results

Rheological Properties

First, the zero-shear viscosity is used as an indicator to understand the material characteristics. In Fig. 1, the complex viscosity is shown over a frequency range from 1 to 500 rad/s.

Figure 1 shows the frequency sweep for the neat materials and the PLA-PHBV based blends at a temperature of 180 °C. All curves show a viscoelastic behavior with a plateau region at low shear rates and shear thinning at higher frequencies. The viscosity at low shear rates is representing the zero-shear viscosity. In these measurements, the neat PLA showed the highest viscosity decreasing with increasing PHBV content. The transition from the zero-shear plateau to the shear thinning region is characterized by the relaxation time. At this transition, the deformed polymer chains cannot relax back to the initial state and therefor the shear thinning becomes prominent. Additionally, the data were modeled according to Carreau-Winter and the parameters are included in the additional information.

Besides the viscosity curves, storage modulus, loss modulus and loss factor provide additional insights into the polymer behavior. The corresponding measurements are plotted in Fig. 2.

In Fig. 2a, the storage modulus for all blends is shown at a temperature of 180 °C. PLA shows the higher storage modulus at high frequencies. The increase of PHBV content decreases the level. At low frequencies, the neat PLA curve is crossed by the measured blend curves. At these low frequencies, the influence of high relaxation times is more pronounced which gives deeper insights into the structure of the polymer [53]. For the neat polymers, the shapes of the curves are congruent and show a typical behavior for linear polymers. Although, the blends show a different G′ behavior compared to the neat polymers. The slope of G′ is decreasing with increasing PHBV content, indicating an increasing elastic behavior at lower frequency levels. Similar results have been seen by [54]. This flattening G′ curve can be related to the interfacial tension in multiphase/immiscible polymer blends [55, 56]. For the lowest shown frequencies in Fig. 2a, the curves containing PHBV show a shoulder which is more pronounced at high PHBV levels. This increase in elastic response relates to the morphology of the polymer blend [57]. Often this phenomenon is called second plateau which is caused by the deformation of droplets of PHBV and their relaxation behavior [58, 59]. In [49] the Droplet morphology was proven via IR-AFM measurements for these blends. During shear stress, the droplets are deformed and store additional energy leading to an increase in G′. Due to the long relaxation times of immiscible polymer blends, this phenomenon can only be detected at low frequency levels [60]. Comparing all blends, the sample containing 20 wt% of PHBV shows the highest storage modulus followed by 10 wt%, 30 wt% and 40 wt% of PHBV. Here the interaction is most pronounced for the 80/20 blend due to an

Fig. 1 Complex shear viscosity over frequency at 180 °C at a strain of 10%
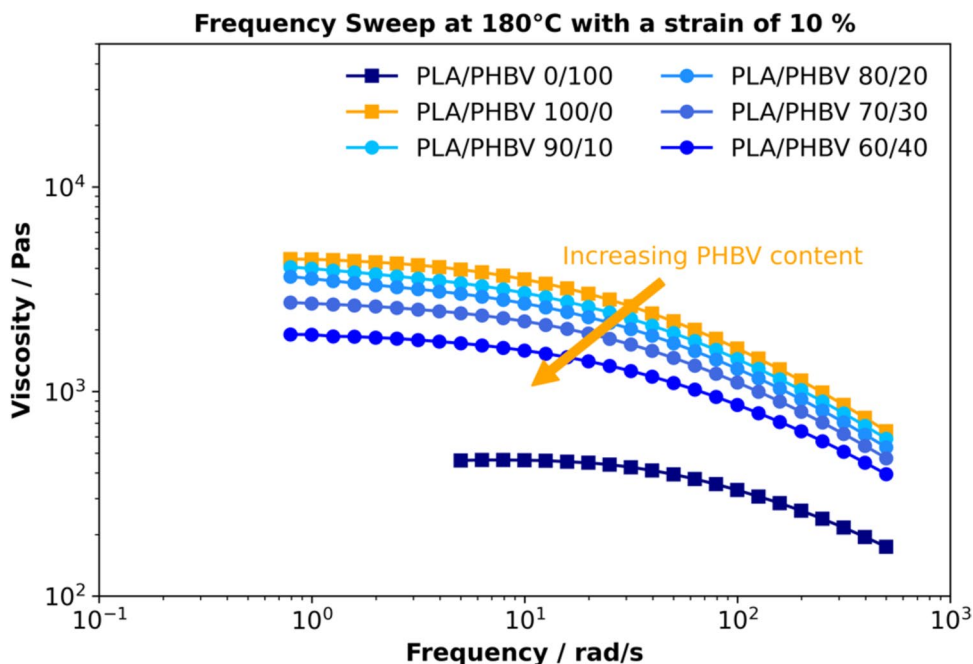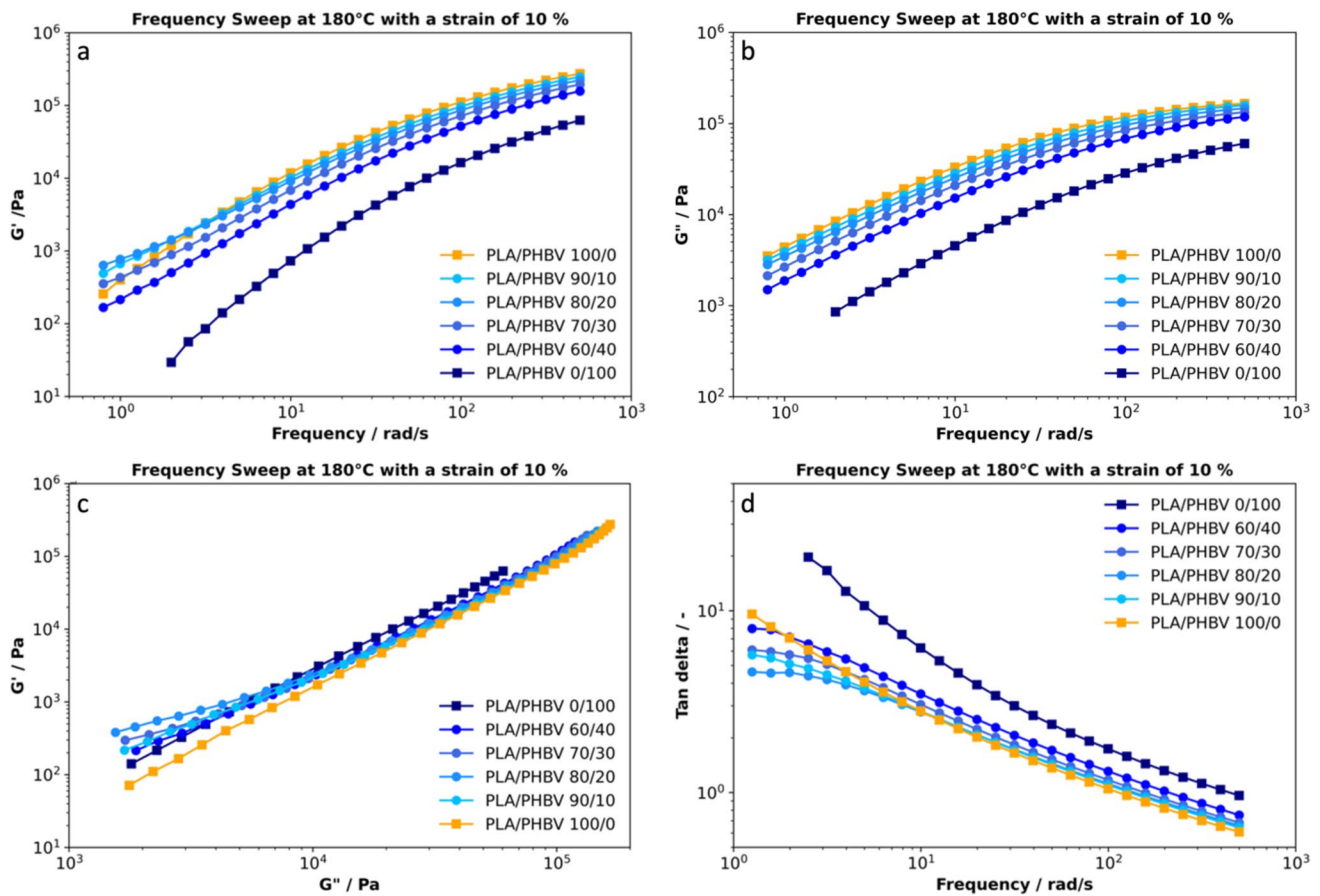
Fig. 2 **a** Storage modulus G over frequency ′, **b** loss modulus over frequency, **c** storage modulus over complex modulus, **d** loss factor over frequency at a temperature of 180 °C for all blend structures

"optimum" in droplet size and interspatial interaction. For linear polymers the storage modulus and the loss modulus follow $G' \sim \omega^2$ and $G'' \sim \omega^1$ at low frequencies [53, 61]. As previously described, the storage modulus does not follow this approximation due to the flattening of the curve.

With increasing PHBV content, the loss modulus is decreasing resulting in a lower viscosity of these blends compared to the neat PLA. The miscibility or immiscibility of polymer blends can be determined by plotting G′ vs G″ [62, 63]. For homopolymers, miscible or compatible polymers and polymer systems, the correlation of G′ vs G″ is linear. Immiscible polymer blends derivate linearity. Additionally, it should be noticed, that the rheological properties depend on the morphological state. As long as the blend morphology does not change, the correlation between G′ and G″ are independent from blend composition [62]. In Fig. 2c G′, is plotted vs. G″ which is also called Han plot [64]. As expected, the neat materials show a linear dependency of storage and loss modulus. The PLA/PHBV blends show a nonlinear behavior, especially at low G′/G″ values.

The shape of the curve can be explained by the increasing G′ at low frequencies due to the shape relaxation of the blend droplets. The tan delta is a very important value to describe the viscoelastic behavior [65]. If this value is equal to 0, the system is ideal elastic and the higher tan delta the more pronounced is the viscous behavior [64]. The tan delta is represented by the ratio between G″ and G′, which is often referred to loss factor. For polymer blends without any structure, the tan delta should decrease monotonous with increasing frequency. Another shape of the curve shows a changed viscoelastic behavior. In Fig. 2d, the loss factor for PLA, PHBV as well as for the blends are plotted as a function of frequency. The neat polymers show the expected decreasing behavior. At high frequency levels, the polymer blends with higher PHBV content show less elastic behavior. At high frequencies, the slope of the curves is decreasing, showing a higher elastic response compared to the neat materials. This behavior of the loss factor shows the immiscibility of the polymer blends, similar to the Han plot and the storage modulus over frequency. This can be seen in the flattening

of the loss factor at low frequencies. At the lowest frequency measured, the sample containing 80 wt% of PLA shows the highest elasticity followed by the blends containing 10 wt%, 30 wt% and 40 wt% of PHBV.

From the oscillatory shear test, it can be concluded that the viscosity is decreasing with higher PHBV content. Moreover, the storage modulus does not follow the relation of $G' \sim \omega^2$ which indicates the immiscibility of the blend due to droplet relaxation processes. This was also confirmed by the so-called Han plot. A closer look at the individual curves reveals that the properties do not rise or fall monotonically with the blend content. It shows that the blend with a ratio of 80:20 has the highest elasticity indicating the highest stored energy due to the droplet deformation. The elasticity is decreasing as follows 90:10, 70:30 and 60:40.

Non-isothermal Crystallization Behavior

To understand the crystallization behavior of PLA and the influence of PHBV, rheological and thermal methods were used. For this purpose, all mixtures were cooled at 5 K/min in a plate-plate rheometer and in a DSC. The cooling ramp was chosen to ensure good temperature control, high resolution for all instruments and direct comparability between the methods.
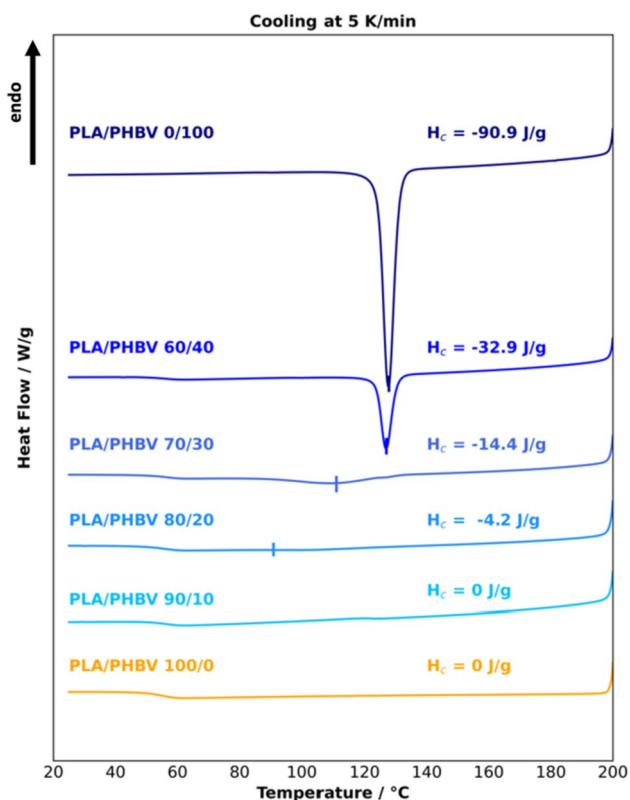

Fig. 3 DSC thermogram of PLA, PHBV and PLA/PHBV blends at a cooling rate of 5 K/min

Figure 3 shows the DSC measurements for all materials used.

The DSC thermogram shows that PHBV crystallizes in a range of 130–120 °C and exhibits a high enthalpy of crystallization and a narrow crystallization peak. In comparison, PLA shows no crystallization peak at the same cooling rates. The combination of PHBV and PLA leads to a different crystallization behavior. The blend containing 10 wt% PHBV does not crystallize in DSC. This suggests that PLA inhibits the crystallization of the PHBV phase. Steric hindrance could be the reason here. When more PHBV is added, the DSC shows a very low degree of crystallization with a peak at about 90 °C. Based on neat PHBV, an enthalpy of crystallization of about 18 J/g is expected by the mixing rule. Since the enthalpy is about 4.2 J/g, steric hindrance is still pronounced. The blends containing 30 wt% and 40 wt% result in more pronounced crystallization, approaching the linear rule of mixture. However, all samples containing both materials show less pronounced crystallization, indicating that the PLA inhibits crystallization and reduces the overall crystallinity upon cooling. This altered crystallization behavior also affects the foaming of the beads, although the cooling rates are significantly higher. The altered crystallization behavior also affects the rheological behavior. To understand this behavior in detail, the same cooling rate was applied to all compounds in a plate-plate rheometer to show this influence. To illustrate the influence, the complex viscosity is plotted as a function of temperature. The results are shown in Fig. 4.

Samples were cooled from 200 to 50 °C for 5 K/min to determine the effect of crystallization on complex viscosity. As shown earlier, the complex viscosity decreases with increasing PHBV content. Thus, the PHBV exhibits the lowest viscosity. As the temperature decreases, the viscosity does not change as much, but at a temperature of 125 °C it increases enormously until contact with the rheometer is lost at 118 °C. Crystallization thus takes place in this temperature range, as it does in the DSC measurements. This increase in complex viscosity is also present in the samples with 40 and 30 wt% PHBV. However, the increase is less pronounced at lower PHBV content, and the samples do not lose contact. Comparing the shape of the curves for pure PLA, PLA + 10 wt% PHBV and PLA + 20 wt% PHBV, a similar behavior can be seen. The increase in viscosity is based on the reduced temperature for pure PLA and PLA + 10 wt% PHBV. Based on the differently shaped curve for PLA + 20 wt% PHBV, crystallization occurs during the cooling process. This is evident at temperatures of about 75 °C, where the curve for PLA + 20 wt% PHBV crosses the curve for PLA + 10 wt% PHBV. This behavior is in line with the DSC results and thus supports the phenomena described.

Fig. 4 Complex viscosity of PLA, PHBV and PLA/PHBV Blends at a temperature sweep test at a cooling rate of 5 K/min
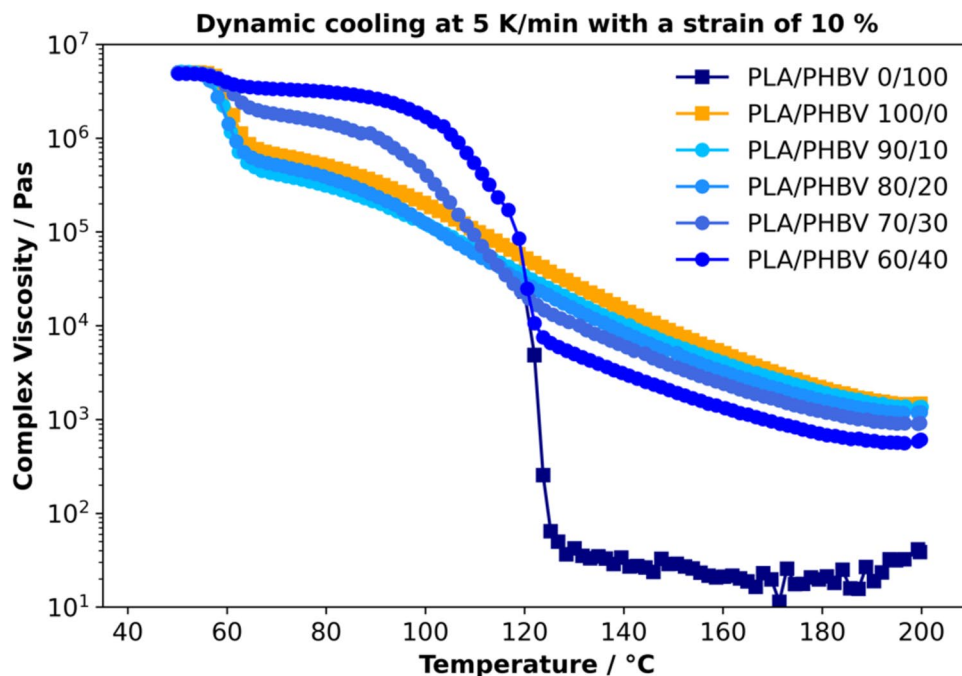
Table 1 Overview of relevant foaming parameters for bead foam extrusion with a die size of 2.8 mm

Material	CO_2 content/%	Die temperature/°C	Die pressure/bar
PLA/PHBV 100/0	6	160	185
PLA/PHBV 90/10	6	160	153
PLA/PHBV 80/20	6	160	132
PLA/PHBV 70/30	6	160	101
PLA/PHBV 60/40	6	160	81

Bead Foaming Behavior

The effect of PHBV on the rheological properties of PLA was studied in detail to provide insights into the foaming behavior. Bead foaming was performed with identical compositions used in the rheological studies. To compare the foaming performance between the different compositions, all materials were processed at similar conditions. A blowing agent content of 6 wt% CO_2 and a foaming temperature (melting temperature) of approx. 135 °C were selected. The temperatures varied by ± 1 K, since the different material compositions showed different rheological properties. The different rheological properties caused different shear forces and friction which leads to additional thermal energy during processing. However, in addition to the melting temperature, the pressure level was also affected by the change in polymer

composition. As shown by the rheological measurements, the viscosity is reduced by adding PHBV. This effect was verified by the pressure profile when the material composition was changed from PLA to PHBV. The addition of PHBV leads to a decrease in pressure, which is known to affect the foaming performance. The influence of PHBV on the resulting pressure is shown in Table 1.

The density achieved for PLA was 63 kg/m³. PHBV was then added stepwise, keeping the throughput constant at 8 kg/h to ensure comparability. It was found that adding PHBV decreased the pressure profile due to the lower viscosity values. This behavior agrees well with the shear rheological results shown in Fig. 1. The pressure decreases almost linearly by 20 to 30 bar per 10 wt%. Besides other influences factors, this pressure drop changes the foaming behavior, and the resulting density is increased. Due to the lower pressure, the overall pressure drop rate decreases, limiting nucleation and expansion. The pressure could not be increased without changing other parameters, why the study focused only on the impact of the material composition on the process and on the foaming behavior. Besides the reduced pressure, the crystallization, the sorption, and the diffusion rates are also changed and influence the foaming behavior. Prior to analyze the morphology the resulting beads are shown in Fig. 5. From the size of the particles one can estimate the differences in density. An analysis of the particle size is included in the additional information. PLA resulted in the lowest densities and increased with PHBV content. The reasons could be the increased crystallization due to the PHBV phase; the reduced pressure drop or the

Fig. 5 Optical image of resulting bead foams
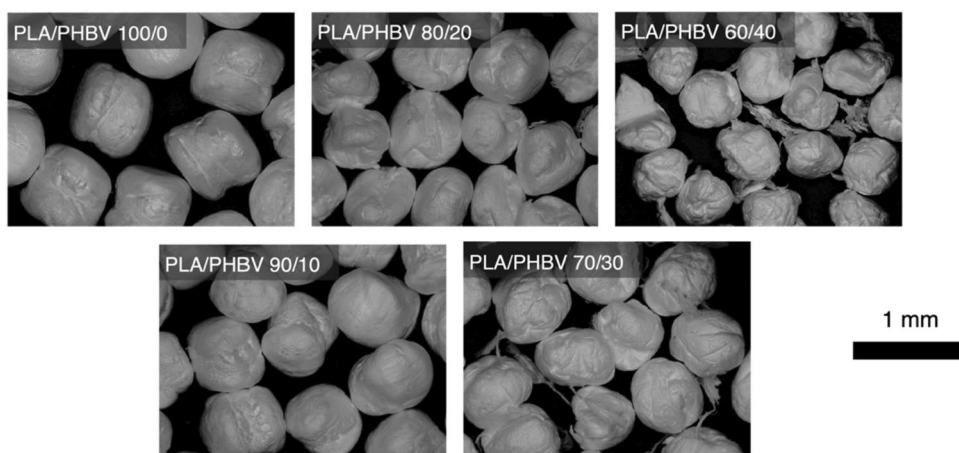
lower sorption behavior of PHBV. In [49] it was shown, that PLA has a higher CO_2 solubility at room temperature compared to PHBV whereas it is expected that this trend is also present here.

For the PLA sample shown in Fig. 6a, small cells can be seen in the range below 60 μm with an average cell size of 36 μm at a density of 63 kg/m^3. Closer analysis of the cells reveals small holes indicating cell breakage during foaming, which leads to a high content of open cells. The cell density for pure PLA is about 1.1×10^7 cells/cm^3. The addition of 10 wt% PHBV (Fig. 6b) results in less nucleation and higher densities. Adding PHBV changes the sorption, crystallization, and rheological properties. The higher PHBV content leads to lower pressure profile and pressure drop rates. It is known from literature that lower pressure and pressure drop rates lead to lower densities. From the rheological investigations in Fig. 4 it seems that the crystallization does not play a big role for 10 or 20 wt% PHBV. Despite the addition of PHBV, the density of cell nucleation decreased, but the mean cell size remained similar at 37 μm with a slightly wider cell size distribution. The decrease in pressure drop reduces both cell density and nucleation compared to pure PLA. The addition of 20 wt% PHBV showed similar trends as it can be seen in Fig. 6c. The density was increased to 86 kg/m^3, the average cell size increased to 53 μm, and the cell density and nucleation density decreased. In addition, the cell size distribution broadened. The blend with 70 wt% PLA and 30 wt% PHBV showed a slightly different trend. Although the density was increased to 96 kg/m^3, the mean cell size decreased from 53 to 36 μm. At this concentration, the nucleation effect of PHBV comes into play. Since PHBV crystallizes faster, it might act as a nucleation site during foaming and increases the total number of cells, resulting in a smaller mean cell size. This is evidenced by

checking the cell density of 1.1×10^7 cells/cm^3 for 30 wt% PHBV compared to 0.4×10^7 cells/cm^3 for 20 wt% PHBV.

A similar trend is shown for the nucleation density. Here, it should be mentioned that two effects interact: (i) the reduced nucleation due to a lower pressure drop and (ii) the increasing nucleation due to the crystallization of PHBV. One hand the PHBV is crystallizing faster than PLA and on the other side the PHBV might crystallize during the processing in the extruder because the temperature profile in the end of the extrusion line is lower than the melting range of PHBV. At a PHBV concentration of 40 wt%, the density increases to 244 kg/m^3, which fits perfectly with the previous results for all other blend contents. Looking at the cell structure, a similar trend as for 30 wt% PHBV can be observed— a decrease in total cell size and cell size distribution. Here, it should be emphasized that this is not necessarily related to the nucleating effect of PHBV on the PLA phase. The cell and nucleation density are increased compared to the sample with 30 wt% PHBV. Thus, fewer cells were nucleated and the effect of pressure on cell nucleation was more pronounced than the crystallization of PHBV. Therefore, the lower mean cell size can be explained by the higher density of the foam.

The morphologies in Fig. 6 provide an overview of all the important features of the bead foams produced. However, to allow a value-based comparison, the information's are analyzed and summarized is compiled in Fig. 7, which makes it easier to see the influence of the blend ratio.

From Fig. 7 one can see that the density is increasing continuously with the increase in PHBV. The cell size is in general decreasing, except at a blend ratio of 20 wt% of PHBV. The cell density does not change tremendously, and the nucleation density is decreasing with increasing PHBV content. However, the sample containing 20 wt% of PHBV
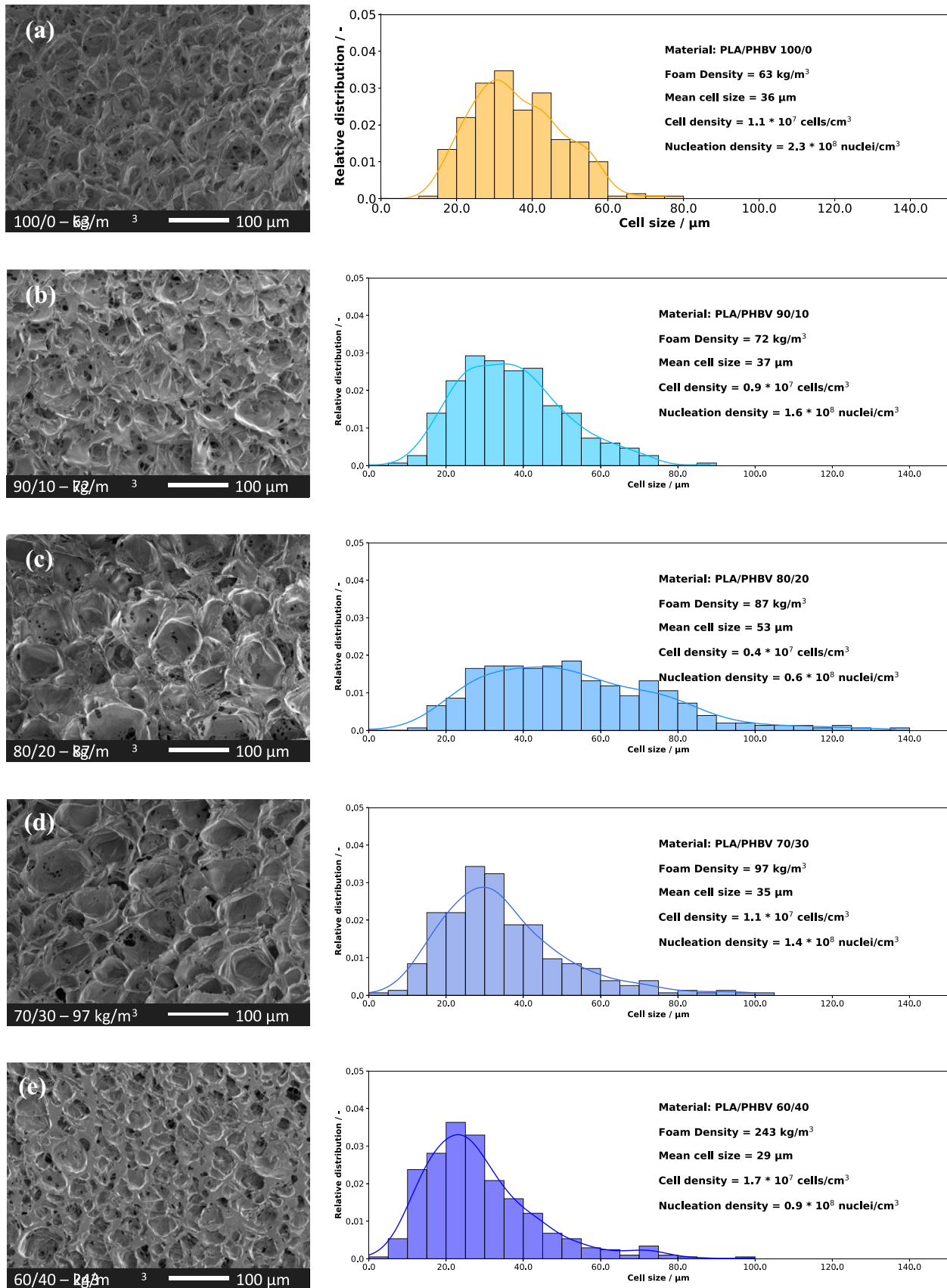
Fig. 6 SEM Images and cell size distribution of the bead foams

Fig. 7 Compilation of density, cell size, cell density and nucleation density as a function of PHBV content in PLA/PHBV bead foams
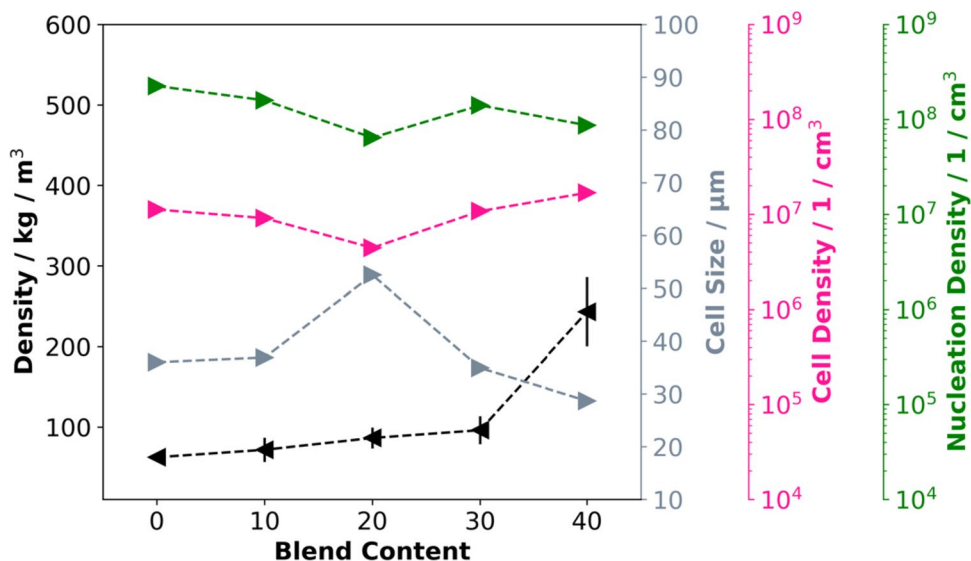

Table 2 Comparison of material composition, the resulting density, and the open cell content

Material	Density	Open cell content
PLA/PHBV 100/0	63 kg/m³	83%
PLA/PHBV 90/10	72 kg/m³	92%
PLA/PHBV 80/20	86 kg/m³	96%
PLA/PHBV 70/30	96 kg/m³	97%
PLA/PHBV 60/40	244 kg/m³	98%

seems be a blend composition where the cells cannot be stabilized and therefore higher cell sizes are reached.

The SEM images provide more insight into foaming behavior. For all foams, small holes can be seen in the cell walls, indicating cell rupture during foaming. The reason might be the low melt properties of the investigated blends, resulting in a low resistance to cell rupture and thus increased open cell content. Additionally, the PHBV might act as foreign substance initiating cell rupture. Table 2 gives an overview of the material composition, densities, and open cell content. Here, the open cell content is generally high

Fig. 8 First heating cycle of different PLA based bead foams
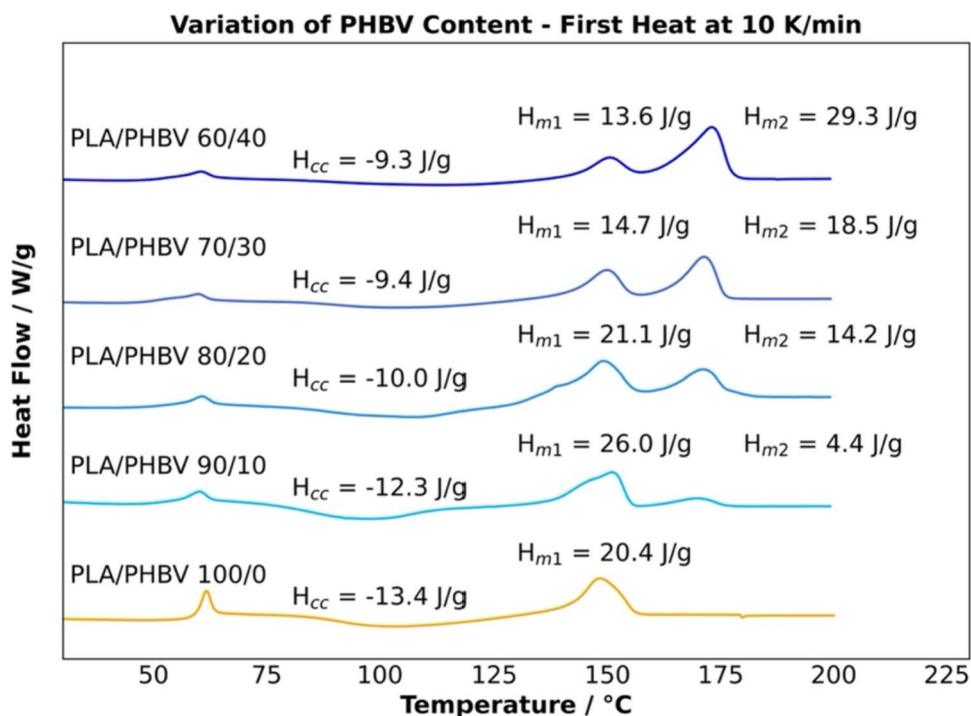
with values above 82% and increases with increasing PHBV content.

To investigate the bead properties, the thermal properties have been analyzed to determine the crystallinities of various samples. Figure 8 shows the thermograms for all produced PLA bead foams for all material compositions. Here it needs to be mentioned that the first heat was selected to be analyzed since this represents the properties of the bead foams. The second heat would show the material properties, which was described elsewhere [49].

It can be seen from Fig. 8, that the glass transitions temperature does not significantly change with the blend composition, which shows the immiscibility of the blend system. The corresponding values from the DSC measurements including the cold crystallization, and melting enthalpies are shown in the supplementary information's. The pure PLA exhibits a pronounced cold crystallization peak and an overall low enthalpy of fusion of 7.0 J/g. Comparing this enthalpy with PLA/PHBV 90/10, the cold crystallization is lower, the overall enthalpy is higher, and a higher melting peak at 170 °C corresponding to the PHBV phase is visible. Further increasing the PHBV fraction leads in increasingly more pronounced melting peaks, due to more crystallizable PHBV. The PLA content is lower, which is mainly responsible for the cold crystallization. However, the melting peak of PLA increases up to a PLA/PHBV ratio of 80/20. This suggests that the PHBV supports the crystallization of PLA even at low concentrations. Therefore, more PLA may crystallize during cooling and heating in DSC. At concentrations of 30 and 40 wt%, the enthalpy for the low melting peak starts to decrease and the enthalpy of the high melting peak starts to increase. This can be related to the blending ratios, as less PLA is available to form the low-melting peak and more PHBV is available to form the high-melting crystals.

An overview about the relative crystallinity of each phase is given in Table 3. Here the Peak corresponding to PLA was taken and the cold crystallization was subtracted. Afterwards the relative crystallinity was determined taking the blend ratio and the 100% crystallinity into account. For the PHBV phase the melting peak of PHBV was used. The used heat

of fusion for 100% crystalline PLA was 93 J/g [66–68] and for PHBV 146 J/g [69–71]

One can see that the PLA is slightly crystallizing without PHBV, while PHBV shows quite high relative crystallinities in all blends. Only for the blend containing 10% of PHBV the relative crystallinity of PHBV is below 40%. The reason could be that the PHBV phase is dispersed in the PLA matrix and needs to agglomerate to crystallize. Due to fine dispersed fractions the crystallization might be restricted but is still pronounced. Here, it needs to be mentioned, that the PHBV can crystallize after the extrusion line as well as during the extrusion process since the temperatures are lower than the melting range of PHBV.

The change in crystallinity with the blend ratio can be explained by the mobility of the polymers. Here the viscosity as well as the crystallization is affecting the chain mobility. The high crystallinity of PHBV restricts the chain mobility so that the PLA phase is restricted in its mobility and the crystal growth is limited. Additionally, the higher the PHBV phase, the higher is the potential contact area between the two phases, so that this results in a sterical hindrance. According to the results it seems that the PLA phase can crystallize easier up to a PHBV content of 20 wt%. At a PHBV content higher than 30 wt% the amount of PHBV crystals seems to restrict the chain mobility so that the crystal growth is limited. To sum this up, there are two effects by increasing the PHBV content (i) the increase in crystallinity by PHBV due to lower viscosities and more nucleating points and (ii) decrease in crystallinity due to an increasing contact area between PLA and PHBV.

Conclusion

In conclusion, in this study PLA and PLA/PHBV bead foams, demonstrating that an increase in PHBV content led to a reduction in the pressure profile during the manufacturing process, aligning well with the shear rheological findings, were successfully produced. The rheological properties were also shown to correlate with the pressure profile during foam extrusion. Moreover, the increase in PHBV concentration was found to result in higher foam density, with potential effects on cell size, density, and nucleation. Factors such as lower pressure drop and increased crystallization of the PHBV phase may contribute to the observed lower density. However, it is challenging to discern the individual influences of rheology and crystallization, making it difficult to definitively attribute the observed effects. Ultimately, in the study a range of bead foam densities from 63 to 244 kg/m^3, with cell densities of approximately 1×10^7 cells/cm^3 and cell sizes as small as 29 μm were achieved. Future research

Table 3 Relative crystallinity of the PLA and PHBV phase from Fig. 8

Composition	Crystallinity PLA phase/%	Crystallinity PHBV phase %
PLA/PHBV 60/40	7.7	50.2
PLA/PHBV 70/30	8.1	42.2
PLA/PHBV 80/20	14.9	48.6
PLA/PHBV 90/10	16.4	30
PLA/PHBV 100/0	7.5	0

should focus on evaluating the weldability of these bead foams to assess their potential relative to other materials in similar applications.

Declarations

References

1. Kuhnigk J, Standau T, Dörr D et al (2022) Progress in the development of bead foams—a review. J Cell Plast 58:707–735. https://doi.org/10.1177/0021955X221087603

2. Raps D, Hossieny N, Park CB et al (2015) Past and present developments in polymer bead foams and bead foaming technology. Polymer (Guildf) 56:5–19. https://doi.org/10.1016/j.polymer.2014.10.078

3. Standau T, Zhao C, Castellón SM et al (2019) Chemical modification and foam processing of polylactide (PLA). Polymers (Basel). 11:306. https://doi.org/10.3390/polym11020306

4. Nofar M, Ameli A, Park CB (2015) A novel technology to manufacture biodegradable polylactide bead foam products. Mater Des 83:413–421. https://doi.org/10.1016/j.matdes.2015.06.052

5. Nofar M (2013) Expanded PLA bead foaming: analysis of crystallization kinetics and development of a novel technology. University of Toronto, Toronto

6. Brütting C, Dreier J, Bonten C et al (2021) Amorphous polylactide bead foam-effect of talc and chain extension on foaming behavior and compression properties. J Renew Mater 9:1859–1868. https://doi.org/10.32604/jrm.2021.016244

7. Dreier J, Brütting C, Ruckdäschel H et al (2021) Investigation of the thermal and hydrolytic degradation of polylactide during autoclave foaming. Polymers (Basel) 13:2624. https://doi.org/10.3390/polym13162624

8. Nofar M, Ameli A, Park CB (2015) Expanded polylactide bead foaming—a new technology. AIP Conf Proc. https://doi.org/10.1063/1.4918400

9. Nofar M, Ameli A, Park CB (2015) Development of polylactide bead foams with double crystal melting peaks. Polymer (Guildf) 69:83–94. https://doi.org/10.1016/j.polymer.2015.05.048

10. Brütting C, Standau T, Meuchelböck J et al (2023) A review on semi-crystalline polymer bead foams from stirring autoclave: processing and properties. E-Polymers. https://doi.org/10.1515/epoly-2023-0092

11. Standau T, Hädelt B, Fafara M et al (2019) Development of a bead foam based on the engineering polymer polybutylene terephthalate. AIP Conf Proc. https://doi.org/10.1063/1.5084836

12. Weingart N, Raps D, Kuhnigk J et al (2020) Expanded polycarbonate (EPC)—a new generation of high-temperature engineering bead foams. Polymers (Basel) 12:2314. https://doi.org/10.3390/polym12102314

13. Mihai M, Huneault MA, Favis BD (2010) Rheology and extrusion foaming of chain-branched poly(lactic acid). Polym Eng Sci 50:629–642. https://doi.org/10.1002/pen.21561

14. Liu W, Li H, Wang X et al (2013) Effect of chain extension on the rheological property and thermal behaviour of poly(lactic acid) foams. Cell Polym 32:343–368. https://doi.org/10.1177/026248931303200602

15. Wang J, Zhu W, Zhang H et al (2012) Continuous processing of low-density, microcellular poly(lactic acid) foams with controlled cell morphology and crystallinity. Chem Eng Sci 75:390–399. https://doi.org/10.1016/j.ces.2012.02.051

16. Corre YM, Maazouz A, Duchet J et al (2011) Batch foaming of chain extended PLA with supercritical CO2: influence of the rheological properties and the process parameters on the cellular structure. J Supercrit Fluids 58:177–188. https://doi.org/10.1016/j.supflu.2011.03.006

17. Standau T, Castellón SM, Delavoie A et al (2019) Effects of chemical modifications on the rheological and the expansion behavior of polylactide (PLA) in foam extrusion. E-Polymers 19:297–304. https://doi.org/10.1515/epoly-2019-0030

18. Mihai M, Huneault MA, Favis BD et al (2007) Extrusion foaming of semi-crystalline PLA and PLA/thermoplastic starch blends. Macromol Biosci 7:907–920. https://doi.org/10.1002/mabi.200700080

19. Li D, Liu T, Zhao L et al (2011) Foaming of poly(lactic acid) based on its nonisothermal crystallization behavior under compressed carbon dioxide. Ind Eng Chem Res 50:1997–2007. https://doi.org/10.1021/ie101723g

20. Standau T, Long H, Castellón SM et al (2020) Evaluation of the zero shear viscosity, the D-content and processing conditions as foam relevant parameters for autoclave foaming of standard polylactide (PLA). Materials (Basel) 13:1371. https://doi.org/10.3390/ma13061371

21. Takada M, Hasegawa S, Ohshima M (2004) Crystallization kinetics of poly(L-lactide) in contact with pressurized CO_2. Polym Eng Sci 44:186–196. https://doi.org/10.1002/pen.20017

22. Nofar M, Tabatabaei A, Ameli A et al (2014) Comparison of melting and crystallization behaviors of polylactide under

high-pressure CO_2, N_2, and He. AIP Conf Proc 1593:320–323. https://doi.org/10.1063/1.4873791

23. Nofar M, Tabatabaei A, Ameli A et al (2013) Comparison of melting and crystallization behaviors of polylactide under high-pressure CO_2, N_2, and He. Polymer (Guildf) 54:6471–6478. https://doi.org/10.1016/j.polymer.2013.09.044

24. Raps D, Köppl T, De Anda AR et al (2014) Rheological and crystallisation behaviour of high melt strength polypropylene under gas-loading. Polymer (Guildf) 55:1537–1545. https://doi.org/10.1016/j.polymer.2014.01.036

25. Takada M, Ohshima M (2003) Effect of CO_2 on crystallization kinetics of poly(ethylene terephthalate). Polym Eng Sci 43:479–489. https://doi.org/10.1002/pen.10039

26. Dörr D, Standau T, Castellón SM et al (2020) Rheology in the presence of carbon dioxide (CO2) to study the melt behavior of chemically modified polylactide (PLA). Polymers 12:1108. https://doi.org/10.3390/POLYM12051108

27. Brütting C, Dreier J, Bonten C et al (2022) Glass transition of PLA-CO 2 mixtures after solid-state saturation. J Cell Plast 58:917–931. https://doi.org/10.1177/0021955X221144543

28. Zhou M, Zhou P, Xiong P et al (2015) Crystallization, rheology and foam morphology of branched PLA prepared by novel type of chain extender. Macromol Res 23:231–236. https://doi.org/10.1007/s13233-015-3018-0

29. You J, Lou L, Yu W et al (2013) The preparation and crystallization of long chain branching polylactide made by melt radicals reaction. J Appl Polym Sci 129:1959–1970. https://doi.org/10.1002/app.38912

30. Nofar M, Zhu W, Park CB et al (2011) Crystallization kinetics of linear and long-chain-branched polylactide. Ind Eng Chem Res 50:13789–13798. https://doi.org/10.1021/ie2011966

31. Wang L, Wang YN, Huang ZG et al (2015) Heat resistance, crystallization behavior, and mechanical properties of polylactide/nucleating agent composites. Mater Des 66:7–15. https://doi.org/10.1016/j.matdes.2014.10.011

32. Battegazzore D, Bocchini S, Frache A (2011) Crystallization kinetics of poly(lactic acid)-talc composites. Express Polym Lett 5:849–858. https://doi.org/10.3144/expresspolymlett.2011.84

33. Refaa Z, Boutaous M, Rousset F et al (2014) Crystallization kinetics of poly-(lactic acid) with and without talc: optical microscopy and calorimetric analysis. AIP Conf Proc 1593:342–346. https://doi.org/10.1063/1.4873796

34. Huang A, Yu P, Jing X et al (2016) The effect of talc on the mechanical, crystallization and foaming properties of poly(lactic acid). J Macromol Sci Part B 55:908–924. https://doi.org/10.1080/00222348.2016.1217186

35. Hu Y, Sato H, Zhang J et al (2008) Crystallization behavior of poly(l-lactic acid) affected by the addition of a small amount of poly(3-hydroxybutyrate). Polymer (Guildf) 49:4204–4210. https://doi.org/10.1016/J.POLYMER.2008.07.031

36. Albuquerque RQ, Brütting C, Standau T et al (2022) A machine learning investigation of low-density polylactide batch foams. E-Polymers 22:318–331. https://doi.org/10.1515/epoly-2022-0031

37. Maga D, Hiebel M, Thonemann N (2019) Life cycle assessment of recycling options for polylactic acid. Resour Conserv Recycl 149:86–96. https://doi.org/10.1016/j.resconrec.2019.05.018

38. Spierling S, Knüpffer E, Behnsen H et al (2018) Bio-based plastics—a review of environmental, social and economic impact assessments. J Clean Prod 185:476–491. https://doi.org/10.1016/j.jclepro.2018.03.014

39. Spierling S, Venkatachalam V, Mudersbach M et al (2020) End-of-life options for bio-based plastics in a circular economy—status quo and potential from a life cycle assessment perspective. Resources 9:90. https://doi.org/10.3390/resources9070090

40. Khoo HH, Tan RBH (2010) Environmental impacts of conventional plastic and bio-based carrier bags. Int J Life Cycle Assess 15:338–345. https://doi.org/10.1007/s11367-010-0163-8

41. Vea EB, Fabbri S, Spierling S et al (2021) Inclusion of multiple climate tipping as a new impact category in life cycle assessment of polyhydroxyalkanoate (PHA)-based plastics. Sci Total Environ 788:147544. https://doi.org/10.1016/j.scitotenv.2021.147544

42. Pietrosanto A, Scarfato P, Maio DD et al (2021) Development of PLA/PHB blown films with improved performance for food packaging applications. Chem Eng Trans. https://doi.org/10.3303/CET2187016

43. Zembouai I, Bruzaud S, Kaci M et al (2014) Poly(3-hydroxybutyrate-co-3-hydroxyvalerate)/polylactide blends: thermal stability, flammability and thermo-mechanical behavior. J Polym Environ 22:131–139. https://doi.org/10.1007/s10924-013-0626-7

44. Gerard T, Budtova T (2012) Morphology and molten-state rheology of polylactide and polyhydroxyalkanoate blends. Eur Polym J 48:1110–1117. https://doi.org/10.1016/J.EURPOLYMJ.2012.03.015

45. Refaa Z, Boutaous M, Siginer DA (2018) PLA crystallization kinetics and morphology development. Int Polym Process 33:336–344. https://doi.org/10.3139/217.3525

46. Kolstad JJ (1996) Crystallization kinetics of poly(L-lactide-co-meso-lactide). J Appl Polym Sci 62:1079–1091. https://doi.org/10.1002/(SICI)1097-4628(19961114)62:7%3c1079::AID-APP14%3e3.0.CO;2-1

47. Gasmi S, Hassan MK, Luyt AS (2019) Crystallization and dielectric behaviour of PLA and PHBV in PLA/PHBV blends and PLA/PHBV/TiO2 nanocomposites. Express Polym Lett 13:199–212. https://doi.org/10.3144/expresspolymlett.2019.16

48. Lim L-TT, Auras R, Rubino M (2008) Processing technologies for poly(lactic acid). Prog Polym Sci 33:820–852. https://doi.org/10.1016/j.progpolymsci.2008.05.004

49. Brütting C, Dreier J, Bonten C et al (2023) Sustainable immiscible polylactic acid (PLA) and poly(3-hydroxybutyrate-co-3-hydroxyvalerate) (PHBV) blends: crystallization and foaming behavior. ACS Sustain Chem Eng 11:6676–6687. https://doi.org/10.1021/acssuschemeng.3c00199

50. Abdelwahab MA, Flynn A, Chiou B-SS et al (2012) Thermal, mechanical and morphological characterization of plasticized PLA–PHB blends. Polym Degrad Stab 97:1822–1828

51. Abu Aldam S, Dey M, Javaid S et al (2020) On the synthesis and characterization of polylactic acid, polyhydroxyalkanoate, cellulose acetate, and their engineered blends by solvent casting. J Mater Eng Perform 29:5542–5556. https://doi.org/10.1007/S11665-020-04594-3/FIGURES/13

52. Okolieocha C, Raps D, Subramaniam K et al (2015) Microcellular to nanocellular polymer foams: progress (2004–2015) and future directions—a review. Eur Polym J 73:500–519. https://doi.org/10.1016/j.eurpolymj.2015.11.001

53. Tian J, Yu W, Zhou C (2006) The preparation and rheology characterization of long chain branching polypropylene. Polymer (Guildf) 47:7962–7969. https://doi.org/10.1016/J.POLYMER.2006.09.042

54. Gui ZY, Wang HR, Gao Y et al (2012) Morphology and melt rheology of biodegradable poly(lactic acid)/poly(butylene succinate adipate) blends: effect of blend compositions. Iran Polym J (English Ed) 21:81–89. https://doi.org/10.1007/S13726-011-0009-7/FIGURES/4

55. Gramespacher H, Meissner J (1992) Interfacial tension between polymer melts measured by shear oscillations of their blends. Cit J Rheol 36:1127. https://doi.org/10.1122/1.550304

56. Bousmina M (1999) Effect of interfacial tension on linear viscoelastic behavior of immiscible polymer blends. Rheol Acta 38:251–254. https://doi.org/10.1007/s003970050175

57. McCallum TJ, Kontopoulou M, Park CB et al (2007) The rheological and physical properties of linear and branched polypropylene blends. Polym Eng Sci 47:1133–1140

58. Lacroix C, Aressy M, Carreau PJ (1997) Linear viscoelastic behavior of molten polymer blends: a comparative study of the Palierne and Lee and Park models. Rheol Acta 36:416–428

59. Graebling D, Muller R, Palierne JF (1993) Linear viscoelastic behavior of some incompatible polymer blends in the melt. Interpret Data Model Emul Viscoelast Liq Macromol 26:320–329

60. Utracki LA, Sammut P (1988) Rheological evaluation of polystyrene/polyethylene blends. Polym Eng Sci 28:1405–1415. https://doi.org/10.1002/PEN.760282110

61. Mizuno C, John B, Okamoto M (2013) Percolated network structure formation and rheological properties in nylon 6/clay nanocomposites. Macromol Mater Eng 298:400–411. https://doi.org/10.1002/MAME.201200065

62. Chuang HK, Han CD (1984) Rheological behavior of polymer blends. J Appl Polym Sci 29:2205–2229. https://doi.org/10.1002/APP.1984.070290625

63. Han CD, Chuang HK (1985) Criteria for rheological compatibility of polymer blends. J Appl Polym Sci 30:4431–4454. https://doi.org/10.1002/APP.1985.070301118

64. Cui L, Zhou Z, Zhang Y et al (2007) Rheological behavior of polypropylene/novolac blends. J Appl Polym Sci 106:811–816. https://doi.org/10.1002/APP.26515

65. Joshi K, Lee JG, Shafi MA et al (1998) Prediction of cellular structure in free expansion of viscoelastic media. J Appl Polym Sci 67:1353–1368. https://doi.org/10.1002/(sici)1097-4628(19980222)67:8%3c1353::aid-app2%3e3.3.co;2-3

66. Ameli A, Nofar M, Jahani D et al (2015) Development of high void fraction polylactide composite foams using injection molding: crystallization and foaming behaviors. Chem Eng J 262:78–87. https://doi.org/10.1016/j.cej.2014.09.087

67. Fischer EW, Sterzel HJ, Wegner G (1973) Investigation of the structure of solution grown crystals of lactide copolymers by means of chemical reactions. Kolloid-Zeitschrift Und Zeitschrift Für Polym 251:980–990. https://doi.org/10.1007/BF01498927

68. Migliaresi C, Cohn D, De Lollis A et al (1991) Dynamic mechanical and calorimetric analysis of compression-molded PLLA of different molecular weights: effect of thermal treatments. J Appl Polym Sci 43:83–95. https://doi.org/10.1002/app.1991.070430109

69. Barham PJ, Keller A, Otun EL et al (1984) Crystallization and morphology of a bacterial thermoplastic: poly-3-hydroxybutyrate. J Mater Sci 19:2781–2794. https://doi.org/10.1007/BF01026954

70. Srubar WV, Pilla S, Wright ZC et al (2012) Mechanisms and impact of fiber–matrix compatibilization techniques on the material characterization of PHBV/oak wood flour engineered biobased composites. Compos Sci Technol 72:708–715. https://doi.org/10.1016/j.compscitech.2012.01.021

71. Lüpke T, Radusch H-J, Metzner K (1998) Solid-state processing of phb-powders. Macromol Symp 127:227–240. https://doi.org/10.1002/masy.19981270130